side of the model centerline at angle of attack. The exact cause was not determined because of limitations on flow-visualization methods.

The data of Fig. 3 indicate a decrease in base heating with increasing angle of attack, except for the slight increase from $\alpha = 15°$ to $\alpha = 20°$. The increase might be explained by flow attachment occurring along the windward side of the conical afterbody for α near 20°, as reported by other investigators.[3,4] The base heating-rate levels are comparable to the levels previously measured by other investigators for the leeward separated region of the conical afterbody and show the same trend of decreased heating with increased angle of attack (see, e.g., Ref. 4).

Also shown in Figs. 2 and 3 are flight data for $\alpha = 20°$ and the same freestream Reynolds number as the tunnel tests.† For the hypersonic tunnel and flight test conditions, the base phenomena are expected to be primarily dependent on the Reynolds number and not the Mach number because of the "Mach number independence principle"[16] for blunt bodies at hypersonic speeds.[17] As with the tunnel data, the flight data indicate highest heating on the leeward side of the base and minimum heating near the base centerline. The agreement between the tunnel data and flight data is better than might be expected considering the fact that the tunnel model is a much "cleaner" configuration than the actual flight vehicle with its numerous surface cavities and protuberances. However, the results of Ref. 5 also showed no apparent difference in the heat transfer to the leeward conical afterbody with and without surface perturbations.

In conclusion, the results of this investigation have indicated highest heating on the leeward side of the base and a general decrease in base heating with increasing angle of attack. Also, the base heating-rate levels are comparable to levels previously measured for the leeward separated region of the conical afterbody. Finally, flight data for $\alpha = 20°$ and the same Reynolds number as the tunnel tests are in general agreement with the tunnel data and also indicate highest heating on the leeward side of the base.

References

[1] Jones, R. A., "Experimental Investigation of the Overall Pressure Distribution, Flow Field, and Afterbody Heat Transfer Distribution of an Apollo Reentry Configuration at a Mach Number of 8," TM X-813, 1963, NASA.

[2] Jones, J. J. and Moore, J. A., "Shock-Tunnel Heat-Transfer Investigation on the Afterbody of an Apollo-Type Configuration at Angles of Attack Up to 45°," TM X-1042, 1964, NASA.

[3] Lee, G. and Sundell, R. E., "Heat-Transfer and Pressure Distributions on Apollo Models at $M = 13.8$ in an Arc-Heated Wind Tunnel," TM X-1069, 1965, NASA.

[4] Fox, G. L. and Marvin, J. G., "An Investigation of the Apollo Afterbody Pressure and Heat Transfer at High Enthalpy," TM X-1197, 1966, NASA.

[5] Bertin, J. J., "The Effect of Protuberances, Cavities, and Angle of Attack on the Wind-Tunnel Pressure and Heat-Transfer Distribution for the Apollo Command Module," TM X-1243, 1966, NASA.

[6] McDevitt, J. B., Harrison, D. R., and Lockman, W. K., "Measurements of Pressures and Heat Transfer by FM Telemetry From Free-Flying Models in Hypersonic Tunnel Streams," *Proceedings of the First International Congress on Instrumentation in Aerospace Simulation Facilities*, INTERCON, available from P. L. Clemens, VKF/AP, Arnold Air Force Station, Tenn., Sept. 28–29, 1964, pp. 16-1to 16-12; also *IEEE Transactions on Aerospace Electronic Systems*, Vol. AES-2, Jan. 1966, pp. 2–12.

[7] Lockman, W. K., "Free-Flight Base Pressure and Heating Measurements on Sharp and Blunt Cones in a Shock Tunnel," *AIAA Journal*, Vol. 5, No. 10, Oct. 1967, pp. 1898–1900.

[8] Harrison, D. R. and Lockman, W. K., "Heat-Transfer Telemetry From Free-Flight Models in Wind Tunnels—Part 2, Using Thermocouple Sensors," AIAA Paper 68-407, San Francisco, Calif., 1968.

[9] Harrison, D. R. and Lockman, W. K., "Heat-Transfer Telemetry for Models Using Thermocouple Sensors," *Journal of Spacecraft and Rockets*, Vol. 6, No. 1, Jan. 1969, pp. 76–78.

[10] Cunningham, B. E. and Kraus, S., "A 1-Foot Hypervelocity Shock Tunnel in Which High-Enthalpy, Real-Gas Air Flows Can be Generated With Flow Times of About 180 Milliseconds," TN D-1428, 1962, NASA.

[11] Loubsky, W. J., Hiers, R. S., and Stewart, D. A.," Performance of a Combustion Driven Shock Tunnel With Applications to the Tailored Interface Operating Conditions," Third Conference on Performance of High Temperature Systems, Dec. 7–9, 1964.

[12] Marvin, J. G. and Akin, C. M., "Pressure and Convective Heat-Transfer Measurements in a Shock Tunnel Using Several Test Gases," TN D-3017, 1965, NASA.

[13] Hiers, R. S., Jr. and Reller, J. O., Jr., "Analysis of Nonequilibrium Air Streams in the Ames 1-Foot Shock Tunnel," TN D-4985, 1969, NASA.

[14] Stoney, W. E., Jr., "Aerodynamic Heating of Blunt Nose Shapes at Mach Numbers up to 14," RML 58E05a, 1958, NACA.

[15] Boison, J. C. and Curtiss, H. A., "An Experimental Investigation of Blunt Body Stagnation Point Velocity Gradient," *ARS Journal*, Vol. 29, No. 2, Feb. 1959, pp. 130–135.

[16] Hayes, W. D. and Probstein, R. F., *Hypersonic Flow Theory*, Academic Press, New York, 1959.

[17] Dewey, C. F., Jr., "Near Wake of a Blunt Body at Hypersonic Speeds," *AIAA Journal*, Vol. 3, No. 6, June 1965, pp. 1001–1010.

† These flight data are for entry of S/C 101 of Apollo-Saturn Mission 205 and were provided by D. B. Lee of NASA Manned Spaceflight Center.

ICRPG Measurement Uncertainty Model for Liquid Rockets

D. L. Colbert,* B. D. Powell,* and R. B. Abernethy†

Pratt & Whitney Aircraft, Florida Research and Development Center, West Palm Beach, Fla.

A SURVEY of the rocket industry in 1966 showed that, among the twelve companies responding to the survey, at least six different methods of treating measurement errors were in use. The Interagency Chemical Rocket Propulsion Group (ICRPG), through its Experimental Measurements Committee, sponsored the development of the ICRPG Uncertainty Model,[1] which has been accepted as a standard for the liquid rocket industry. The basis for the uncertainty model lies in the nature of measurement error, which has two components: 1) a fixed error called bias, and 2) a random error between repeated measurements which is called precision error. An index of precision error is defined

$$S = \{[\Sigma(X_i - \bar{X})^2]/(N-1)\}^{1/2} \quad (1)$$

where N is the number of measurements (X_i), and $\bar{X}$ is the average of the measurements.

An index of bias is not easily defined. Bias is the fixed, repeatable difference between the measurement and the true value of the parameter (as defined by a standard at the National Bureau of Standards). Because there is no statistic to

Presented as Paper 69-734 at the AIAA 5th Propulsion Joint Specialist Conference, U.S. Air Force Academy, Colo., June 9–13, 1969; submitted May 20, 1969; revision received October 27, 1969. We are indebted to the members of the ICRPG Experimental Measurements Committee for their participation and to Rosenblatt, Ku, and Cameron of the National Bureau of Standards for helpful discussions.

* Assistant Project Engineer.

† Program Manager.

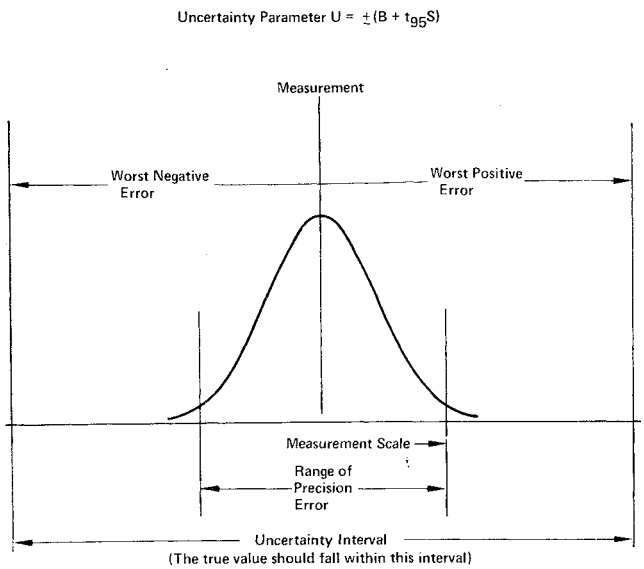

Fig. 1 Measurement uncertainty.

estimate bias which is analogous to the index of precision error, we estimate the upper limit on bias, B, based on engineering judgment and experience.

Uncertainty

For simplicity and for comparisons, we need a single number to express a reasonable limit for error, some function of B and S. Any function of these two numbers must be a hybrid combination of an unknown quantity (bias) and a statistic (precision). However, the need for a single number for uncertainty, U, is so great that we are forced to adopt an arbitrary standard. The following one is most widely used and is recognized and recommended by the National Bureau of Standards (NBS):

$$U = \pm(B + t_{95}S) \tag{2}$$

where U is centered about the measurement (Fig. 1), and t is the 95th percentile point for the two-tailed Students "t" distribution. We have arbitrarily selected $t = 2$ for sample sizes greater than 30.

The ICRPG reporting format is 1) S, calculated from data by Eq. (1); 2) df, the degrees of freedom associated with S; 3) B, the limit of the uncorrected bias of the measurement process; and 4) U, calculated by Eq. (2), beyond which measurement errors would not reasonably fall.

These four numbers provide all the information necessary to describe the measurement error. Uncertainty (U) should never be reported without its components: bias, precision index and degrees of freedom. These components are required for further treatment of error such as the propagation from an engine to a propulsion system. It should be noted that uncertainty, U, can never be propagated. Although uncertainty is not a statistical confidence interval, it is an arbitrary substitute which is probably best interpreted as the largest error we might expect. Under any reasonable assumption for the distribution of bias, the coverage of U is greater than 95%, but this cannot be proved because the distribution of bias is both unknown and unknowable.

Measurement Process

Uncertainty statements are based on a measurement process that must be defined. The process treated by the ICRPG measurement model is the measurement of specific impulse, thrust, and propellant flow for a particular engine model at a given engine manufacturer's facility. The uncertainty will contain precision errors due to variations between installations and calibrations of many measurement instruments for each parameter. This uncertainty will be greater than the uncertainty for comparative tests to measure specific impulse on a single stand for a single firing. The single-stand, single-firing model would assume that most installation-to-installation and calibration-to-calibration errors would be biases rather than precision errors. Biases are ignored in comparative tests.

Table 1 Calibration hierarchy error sources

	Bias	Precision error	Degree of freedom
NBS-interlab standard	b_{11}	s_{11}	df_{11}
Interlab standard-ref. standard	b_{21}	s_{21}	df_{21}
Reference standard-working standard	b_{31}	s_{31}	df_{31}
Working standard-meas. load cell	b_{41}	s_{41}	df_{41}

The definition of the measurement system is prerequisite to defining the mathematical model. We must list all the elemental bias and precision error sources that are being estimated and how they are related to the engine performance parameter. We categorize errors into three groups:

1 Calibration-hierarchy errors

The demanding requirements of missiles and spacecraft had led to the establishment of extensive hierarchies of standards laboratories within industry, traceable to the NBS. As an example, a load cell is calibrated with a portable weigh kit while installed in a thrust stand. The weigh kit is calibrated with a force calibrator which is periodically calibrated in the company laboratory against a proving ring. At infrequent intervals, the ring is recalibrated at the NBS. The five levels in the hierarchy require four comparisons to calibrate the load cell. In each comparison, a precision error and a bias may be involved (see Table 1). The rms precision error, based on precision errors for the four steps in the calibration process, is:

$$S_1 = (s_{11}^2 + s_{21}^2 + s_{31}^2 + s_{41}^2)^{1/2} \tag{3}$$

The df's for the individual s's may be combined using the Welch-Satterthwaite formula to provide an estimate of df_1 for S_1:

$$df_1 = (\Sigma S_{i1}^2)^2/\Sigma(S_{i1}^4/df_{i1}) \quad i = 1,\ldots,4 \tag{4}$$

It is unreasonable to assume that all of the many elemental bias limits are cumulative, because some are positive and some are negative. For this reason, we have arbitrarily adopted an rms bias limit

$$B_1 = (b_{11}^2 + b_{21}^2 + b_{31}^2 + b_{41}^2)^{1/2} \tag{5}$$

Now U_1 may be calculated by Eq. (2).

2 Data acquisition errors

Data are acquired by measuring electrical outputs resulting from forces applied to a strain-gage-type force transducer. Seven error sources associated with data acquisition are: excitation voltage, electrical simulation, signal conditioning, recording device, force transducer, thrust bed mechanics, and environmental effects. Here we define B_2 and S_2 as the rms values of the b_{i2} and s_{i2}, respectively ($i = 1,2,\ldots,7$; the df_{i2} also is defined).

3 Data reduction errors

These errors usually are insignificant. The computer operates on the raw data to produce output in engineering units. The errors in this process stem from 1) calibration curve fits and 2) the computer resolution. Here, $B_3 \equiv (b_{13} + b_{23})^{1/2}$, and $S_3 \equiv (s_{13} + s_{23})^{1/2}$.

Measurement Uncertainty

The foregoing errors are combined to obtain the precision index, bias limit, and uncertainty for the measurement using equations similar to Eqs. (1–5). As an example, let us analyze a Pratt & Whitney Aircraft RL10 rocket engine force measurement. This force measurement makes up a significant portion of the engine thrust; the remainder is due to pressure and area corrections, because the RL10 is designed to fire in the vacuum of outer space. The test stand force measurement is made with a strain gage load cell system. First we consider the errors resulting from the calibration hierarchy. All errors are expressed as percentages of 12,000 lb, and precision errors are one-standard-deviation (1σ) values $b_{11},\ldots,$ b_{41} = 0.002%, 0.002%, 0.011%, and 0.072%; $s_{11},\ldots,s_{41}$ = 0.167%, 0.034%, 0.065%, and 0.031%. From Eqs. (5) and (3), respectively, B_1 = 0.073% and S_1 = 0.186%.

Rather than evaluate each of the errors in the data acquisition and data reduction processes, we have determined the over-all effect of both processes by means of applied load tests. Known forces are applied to the force measurement system with data recorded and reduced to engineering units, utilizing the same procedures employed for acquisition and reduction of run data. In this example, the combined effect of both processes are defined by B_2 and S_2.

Finally, the over-all uncertainty of the force measurement is computed

$$B_F = 0.12\%,\ S_F = 0.20\%,\ U_F = 0.52\%$$

The measured force error must be combined with the nozzle area and pressure correction errors to obtain the RL10 engine thrust uncertainty. This process, called the propagation of error, is described in the following section. The bias and precision index for engine thrust must then be further propagated with propellant measurement errors to obtain the uncertainty for special impulse.

Propagation of Error

We rarely can measure performance parameters directly; usually we make measurements of more basic quantities like temperature, force, pressure, and fuel flow and calculate the performance parameter as a function of the measurements. The error in the measurements is propagated to the parameter through the function. The effect of the propagation may be approximated with Taylor series methods. These transformations are derived and illustrated in Ref. 1.

Reference

[1] *Interagency Chemical Rocket Propulsion Group Handbook for Estimating the Uncertainty in Measurements Made with Liquid Propellant Rocket Engine Systems*, CPIA 180, AD 851127, April 1969.

A Zoom Maneuver for Descent of Roll Modulated Entry Vehicles

W. Frank Staylor*
NASA Langley Research Center, Hampton, Va.

THE weight and complexity of terminal descent systems are often a strong function of the dynamic pressure at deployment.[1,2] Drogue parachutes and/or other types of inflatable decelerators are often employed to reduce the dynamic pressure before deployment of the terminal descent system. In the present Note a flight maneuver is described for a roll-modulated, lifting entry vehicle that can drastically reduce the deployment dynamic pressure.

Received August 18, 1969; revision received October 20, 1969.

* Aero-Space Technologist, Aero-Physics Division. Member AIAA.

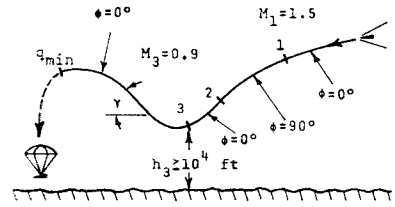

Fig. 1 Zoom maneuver.

An example of a zoom maneuver is shown in Fig. 1 which is initiated at a flight Mach number, M, of 1.5 (point 1) by rolling the vehicle from a bank angle, ϕ, of 0° (lift vector up) to 90° (lift vector horizontal). This causes the flight-path angle γ to decrease and the dynamic pressure q to increase rapidly. At a later flight condition (point 2) the vehicle is rolled back to ϕ = 0°. During this phase of the flight, the vehicle pulls up (γ increases) and M and q decrease rapidly.

The third phase of the zoom maneuver is initiated at M = 0.9 (point 3) with a crew-safety restriction that the altitude, h, be at least 10,000 ft. At this point the vehicle is pitched-up to a high lift attitude, which further increases γ and briefly decreases q to a minimum value which is considerably less than the minimum value that would be obtained without the pitch-up maneuver. A hypersonic, roll-modulated vehicle could be pitched-up with controls deployed at subsonic speeds ($M \leq 0.9$).

In Fig. 2 the flight conditions at the various maneuver points are given for lift drag ratios L/D of 1, 2, and 3 ($M \geq 0.9$) for ranges of ballistic coefficient W/C_DA. The flight conditions in Fig. 2a (M = 1.5) were determined from equilibrium glide flights (ϕ = 0°) beginning at M = 10 and are independent of initial re-entry maneuvers. The discontinuities that occur in Figs. 2b and 2c at $W/C_DA \simeq$ 1000 lb/ft² result from the altitude restriction and would occur at higher values of W/C_DA if M_1 were increased.

In Fig. 3 (top) the minimum dynamic pressures q_{min} are presented for various values of lift coefficient ratio C_{L3}/C_L, each having a corresponding drag coefficient ratio C_{D3}/C_D (C_L and C_D are $M \geq 0.9$ values). These ratios are believed

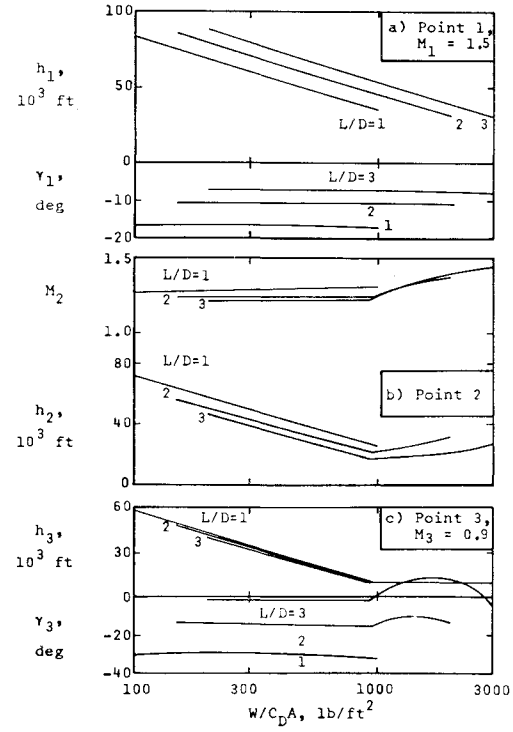

Fig. 2 Flight conditions vs ballistic coefficient for three L/D's.